

Physical properties of the gamma-ray binary LS 5039

Author: Sergi Monserrat Mascaró

Facultat de Física, Universitat de Barcelona, Diagonal 645, 08028 Barcelona, Spain.

Advisor: Josep Maria Paredes Poy

Abstract: We studied the LS 5039 gamma-ray binary in the 0.15-15 GHz range with both simultaneous and non-simultaneous data. From the non-simultaneous data we computed an average spectrum and found that it is best explained by Razin effect with $p = 2.16 \pm 0.04$ and $\nu_R = 0.42 \pm 0.02$ GHz. We obtained two simultaneous spectra for 19 July 2013 and 21 July 2013. The first one was explained by SSA with $p = 1.86 \pm 0.01$ while the second was explained by Razin effect with $p = 2.28 \pm 0.05$ and $\nu_R = 0.44 \pm 0.04$ GHz. Therefore, we conclude that the Razin effect can vary to the point of vanishing completely. This, along with further variations in the spectral index, suggests the source experiences changes in either the synchrotron injection, electron density or magnetic field in the timescale of days and also timescales within the orbital period (3.906 d). Furthermore, the presence of the Razin effect supports a non-accreting pulsar scenario over a microquasar scenario. Finally, we suggest where further research should be directed towards.

I. INTRODUCTION TO GAMMA-RAY BINARIES

Gamma-ray binaries are stellar systems consisting of a massive O/B star and a compact object, either a pulsar or a black hole. These kind of binaries are known to emit non-thermal radiation in a wide range of frequencies, from VHE gamma rays (~ 0.1 TeV), HE gamma rays and X-rays to radio (~ 1 MHz). In addition, radiation is usually modulated by the orbit of the compact object at all frequencies. Though it is not always in phase as, for example, X-ray and VHE emission is modulated in anti-phase with HE emission in the case of LS 5039 (Dubus 2013).

Gamma-ray binaries are scarce as well, with only around half a dozen well-studied cases. Namely, PSR B1259-63, LS 5039, LS I +61 303, HESS J0632+057, 1FGL J1018.6-5856 and LMC P3, with only PSR B1259-63 having a confirmed pulsar (Chernyakova et al. 2019).

High energy emission comes from inverse Compton scattered UV photons from the companion star, but there is some debate as to whether one region or two regions are responsible for separate HE and VHE emission (Zabalza et al. 2013). At radio frequencies, emission is caused by synchrotron. However, the formation of these two parts of the spectrum is under discussion. There are two main competing theories to explain them.

The first one, proposes microquasars as the source. That is, material from the massive star spirals into the compact object and is then accelerated and ejected from the poles in a relativistic jet with radio emission coming from the disk of infalling matter and the shock with the interstellar medium.

The other one states that the companion of the massive star is a young non-accreting pulsar. The pulsar produces a wind that prevents accretion and collides with the companion's wind producing a termination shock that serves as a particle accelerator to generate the non-thermal spectrum. The pulsar has to be young since this con-

ditions are not stable and eventually (typical lifetimes of $\sim 6 \times 10^5$ yr) the pulsar wind cannot overcome accretion and the system transitions to a high mass X-ray binary (HMXB) (Dubus 2013).

The relative ram pressures of the colliding winds will determine the shape of the termination shock, where both pressures are matched. This shock has a bow shape with an angle that closes the more pressure the companion exerts relative to the pulsar. At some point, the pulsar wind can be collimated into a jet or completely engulfed by the companion wind (Dubus 2013).

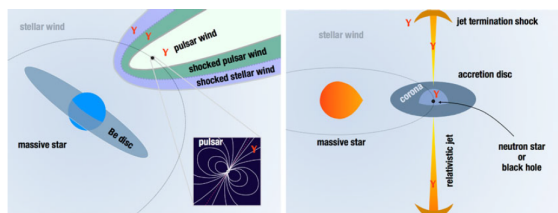


FIG. 1: *Left:* non-accreting pulsar scenario. Both the companion and the pulsar produce winds that collide and form a termination shock that produces non-thermal emission. The Be disc may or may not be present. *Right:* microquasar scenario. Infalling material from the companion forms an accretion disk and part of it is ejected in a relativistic jet. Credit: Dubus (2013)

II. THE LS 5039 SYSTEM

LS 5039 is located in the Scutum constellation at 2.04 ± 0.06 kpc from the Sun (ESA/Gaia/DPAC 2020). It was first discovered in 1997 by Motch et al. as a HMXB and later pointed out as a suspected gamma-ray source in 2000 by Paredes et al. It consists of a $23 M_{\odot}$ young O6.5V star (Casares et al. 2005) and a compact object of unknown nature of $1.4-6.7 M_{\odot}$, the range accounting for different inclinations (13° to 64°) of the orbital plane (Casares et al. 2005). Of the systems mentioned in Section I, LS 5039 has the least eccentric orbit at

$e = 0.24 \pm 0.08$ (Sarty et al. 2011) and the shortest orbital period at 3.906 days (Casares et al. 2005). The system spans ~ 0.3 AU with an apoastron of 0.19 AU and periastron of 0.09 AU whereas other mentioned gamma-ray binaries have orbits in the order of several and up to 10 AU (Dubus 2013). One of the most remarkable features of LS 5039 is the absence of orbital modulation in the radio emission (Chernyakova et al. 2019).

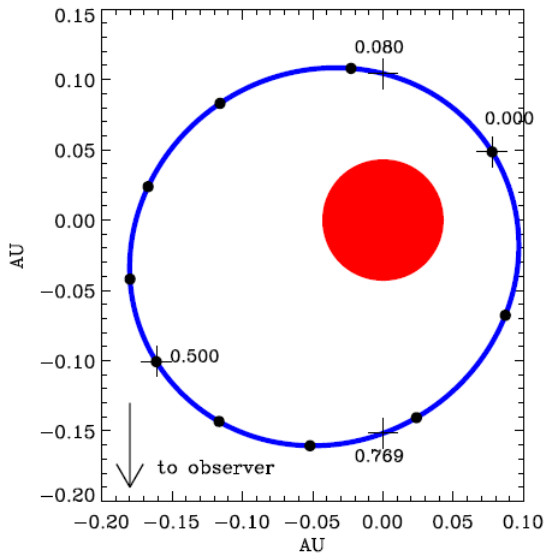


FIG. 2: LS 5039 orbit. Crosses mark the periastron, apoastron and both inferior and superior conjunctions. Dots are spaced in 0.1 orbital phase intervals starting from the perihelion ($\phi = 0$). A full orbit corresponds to $\phi = 1.0$. Credit: Dubus (2013)

Regarding the nature of the compact object, it was first thought that the microquasar scenario was the most likely due to the observation of an elongated radio emission that was interpreted as a pair of relativistic jets (Paredes et al. 2000), a key feature of microquasars, being the resemblance with quasar jets the reason behind the coining of this term. The derived orbital parameters further supported this scenario as the most likely mass for the compact object was found to be $3.7 M_{\odot}$ (Casares et al. 2005).

However, shocked pulsar wind can adopt a similar shape and the orbital study by Casares et al. was not conclusive enough to claim the presence of a black hole. In fact, evidence in favor of the pulsar scenario is getting more experimental support. An argument could be the high gamma-ray luminosity and the timing characteristics of the listed systems in Section I point to a spinning down pulsar as their spectra have similarities with isolated pulsar wind nebulae (PWN) (Dubus 2013). Another argument is that the shocked pulsar wind behaves as a kind of 'cometary tail'. The variability of the source matching the orbital period makes unlikely a microquasar since its relativistic jet isn't expected to change with the orbital phase (Dubus 2013). A more exhaustive and de-

tailed list can be found at Dubus 2013.

The spectral index in the radio frequencies is compatible with synchrotron emission ($\alpha = -0.57 \pm 0.12$) (Marcote et al. 2015) down to ~ 0.5 GHz, where the spectrum changes to a positive index. This indicates the existence of an absorption mechanism. This essay considers SSA (Self-Synchrotron Absorption) and FFA (Free-Free Absorption) as the main mechanisms and the Razin effect as a suppressor of synchrotron emission.

III. MEASUREMENTS

The range of study is 0.15-15 GHz. Observations in the low end of the spectrum (0.154 GHz) are just upper limits as telescopes reach the limit of their sensitivity with some more upper limits also in the 0.235 GHz band.

The measurements compile non-simultaneous observations spanning 20 years gathered from the Very Large Array (VLA), the Giant Metrewave Radio Telescope (GMRT) and the Westerbork Synthesis Radio Telescope (WSRT). The older data (1998-2002) corresponds to higher frequencies (1.4 - 15 GHz) and comes from the VLA while the GMRT and WSRT provide newer data (2004-2013) at a lower range of frequencies (0.154 - 4.8 GHz). This means there is no simultaneity in the observations, but they still allow for an average spectrum to be computed. However, within the data, there are two simultaneous surveys in the 0.154 - 4.8 GHz range corresponding to 19 July 2013 and 21 July 2013. These observations allow to capture the whole 0.154 to 4.8 GHz spectrum in a single night and can provide insight into the variability of the source in the timescale of days.

The observations also cover the whole orbit with gaps at orbital phases $\phi \sim 0.4 - 0.55$ and $\phi \sim 0.85 - 1.0$.

All the measurements used in this essay are available at Marcote et al. 2015

IV. MODELLING OF ABSORPTION MECHANISMS

The absence of orbital modulation in the radio emission is compatible with a spherically symmetric model. For simplicity, isotropy and homogeneity are also assumed.

Since the emission comes from synchrotron, we considered a power law injection of the form

$$n(E)dE = KE^{-p}dE \quad (1)$$

With $p = 1 - 2\alpha$ where α is the spectral index. That will produce a flux density such as

$$S_{\nu} \propto \frac{\Omega J_{\nu}}{4\pi\kappa_{\nu}} (1 - e^{-\kappa_{\nu}r}) \quad (2)$$

according to Longair 2011. Where Ω is the solid angle of the source, r is the radius of the source, J_{ν} is the emissivity and κ_{ν} is the absorption coefficient.

The emissivity of a synchrotron source has the form

$$J_\nu \propto KB^{-(p+1)/2} \nu^{-(p-1)/2} \quad (3)$$

where B is the magnetic field and K the normalization constant

The absorption coefficient can be divided into two contributions, one for each absorption mechanism $\kappa_\nu = \kappa_\nu^{SSA} + \kappa_\nu^{FFA}$ with

$$\kappa_\nu^{SSA} \propto KB^{(p+2)/2} \nu^{-(p+4)/2} \quad (4)$$

$$\kappa_\nu^{FFA} \propto n_e^2 T_w^{-3/2} \nu^{-2} \quad (5)$$

where n_e is the electron density and T_w the stellar wind temperature (Rybicki and Lightman 1979).

As the synchrotron emission does not occur in a complete vacuum but in a plasma, the refractive index $n \neq 1$ and as a consequence light disperses differently depending on the frequency. At the same time, the typical beaming of synchrotron emission depends on the refractive index

$$\Delta\theta \sim 1/\gamma \sim (1 - n^2\beta^2)^{1/2} \quad (6)$$

In a relativistic regime ($\beta \sim 1$), Eq. (6) becomes $\Delta\theta \sim (1 - n^2)^{1/2} \sim \frac{\nu_{plasma}}{\nu}$ and it is easy to see that frequencies similar and lower than the characteristic frequency of the plasma will not be beamed at all (Blackman 2007, Ricotti 2009). This is called Razin effect and it will manifest as a curvature on the spectrum followed by a cutoff.

In order to account for this effect we approximated it modulating S_ν with an exponential factor $e^{-\frac{\nu_R}{\nu}}$ (Marcote et al. 2015). Where $\nu_R = \frac{20n_e}{B}$ is the characteristic frequency below which the flux decreases abruptly (Marcote et al. 2015).

Combining Eq. (4) or (5) with Eqs. (3) and (2) we can model either SSA or FFA with a 3-parametre function to fit

$$S_\nu \propto \frac{P_1}{4\pi} \nu^{f(p)} \left(1 - e^{-P_2 \nu^{g(p)}}\right) \quad (7)$$

Where $f(p) = 5/2$, $g(p) = -(p+4)/2$ for SSA and $f(p) = (5-p)/2$, $g(p) = -2$ for FFA. The parametres being $P_1 = \Omega B^{-1/2}$, $P_2 = KrB^{(p+2)/2}$ for SSA and $P_1 = \frac{\Omega KB^{-(p+1)/2}}{n_e^2 T_w^{-3/2}}$, $P_2 = rn_e^2 T_w^{-3/2}$ for FFA. The addition of Razin effect includes ν_R as a fourth parametre.

If we only want to consider the Razin effect, we have to remove absorption from the source function $S_\nu = \frac{J_\nu}{\kappa_\nu}$. Then there is dependence on 3 parametres: ν_R , p and $P_1 = \Omega KB^{-(p+1)/2}$.

$$J_\nu \propto e^{-\frac{\nu_R}{\nu}} \left(\frac{P_1}{4\pi} \nu^{-\frac{(p-1)}{2}} \right) \quad (8)$$

Where J_ν is no longer the source function but the synchrotron emissivity averaged and integrated over the solid angle (Rybicki and Lightman 1979) and modulated by the Razin effect.

Combining SSA+FFA leads to a more complicated expression with 2 terms adding in the denominator and 2 more in the exponential. We tried a fit for SSA+FFA regardless, but it diverged with nearly vertical asymptotes between points of experimental data so we discarded it.

Since there are only 2 observations at 2.3 GHz, we decided not to use measurements at this frequency in any model as it would not be representative enough. This reduces the experimental data points of the average spectrum to 6.

V. ANALYSIS AND RESULTS

To study the non-simultaneous data we took a weighted average at each frequency. For any given measurement $S_\nu \pm \Delta S_\nu$, the weight is chosen as

$$w = \frac{1}{(\Delta S_\nu)^2} \quad (9)$$

This weighting gives more importance to the more precise measurements and naturally dilutes the effect of measurements with uncertainties comparable to the measured value.

The same procedure can be applied to compute the uncertainty of the average. Assuming the observations are independent

$$\Delta S_\nu = \frac{1}{\sum_i w_i} \sqrt{\sum_i (w_i \Delta S_{\nu_i})^2} \quad (10)$$

But the uncertainties obtained with this method appeared to be too small, so we also considered a much simpler approach

$$\Delta S_\nu = \frac{\sigma_\nu}{\sqrt{N}} \quad (11)$$

Where σ_ν is the standard deviation and N the number of observations at each frequency. We use $\frac{2\sigma_\nu}{\sqrt{N}}$ as error bars.

A simple unweighted average yields a similar spectrum that is within the 2σ error bars as seen in Fig. 3, so no significant differences should be expected from applying different methods. We chose the weighted average for the following calculations. We fitted every model to the data and we found that the approach to the uncertainties in Eq. (10) produced $\chi^2 > 1$ so we changed to Eq. (11).

From Table I we deduce that the average spectrum is best explained by the Razin model. The results of this fit were $\nu_R = 0.42 \pm 0.02$ GHz, $p = 2.16 \pm 0.04$ which yields $\alpha = -0.58 \pm 0.02$ and $P_1 = 1.27 \pm 0.05 \cdot 10^8 \text{ T}^{-(p+1)/2}$.

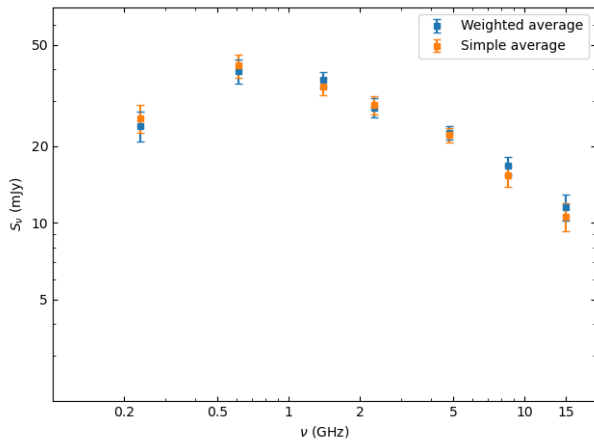


FIG. 3: Comparison between the usage of weighted and un-weighted averages. Error bars are 2σ uncertainties.

Model	χ^2	$\chi^2/d.o.f$
SSA	0.516	0.172
FFA	1.098	0.366
Razin	0.068	0.023
SSA+Razin	0.072	0.036
FFA+Razin	0.070	0.035

TABLE I: Results of the χ^2 test for every model. d.o.f are the degrees of freedom. If the number of parameters to adjust is equal to the number of experimental data points, then d.o.f = 0

The results for the remaining models that include the Razin effect are so similar that they only reaffirm the inability to distinguish the nature of the absorption if present at all.

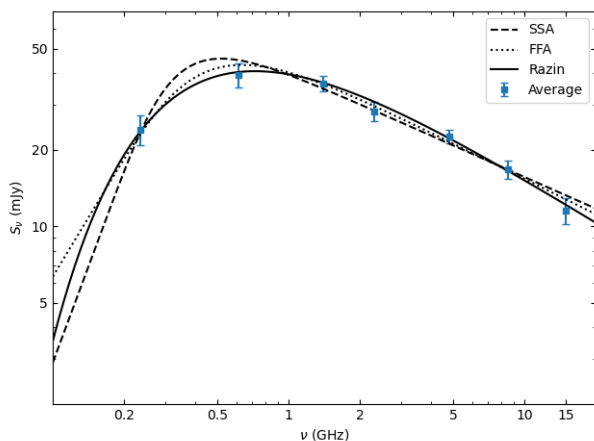


FIG. 4: Averaged spectrum from non-simultaneous data with SSA, FFA and Razin models fitted. Error bars are 2σ uncertainties

The analysis of the two simultaneous spectra had only 4 experimental data points. This meant that any 4-

parametre fit would match the data perfectly ($\chi^2 = 0$) by definition, that is, SSA+Razin or FFA+Razin was going to be the best model almost by default. So the only way to discard these models was if $\nu_R \approx 0$, which meant the Razin effect would be weak or even non-existent.

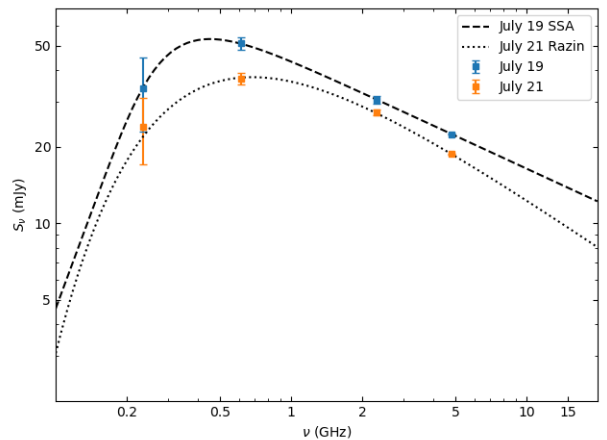


FIG. 5: Spectra for 19 July 2013 with SSA fit and 21 July 2013 with SSA+Razin fit. The Razin effect is responsible for the curvature in the 21 July spectrum. The turnover is at a lower frequency when the Razin effect is not present. Uncertainties are as featured in Marcote et al. 2015.

For the 19 July 2013 data we found that, in fact, $\nu_R \sim 10^{-34}$ GHz, meaning that pure SSA alone could explain the spectrum (Table III). This spectrum managed to constrain the values of P_1 and P_2 (Table II).

Spectrum	$P_1(\text{T}^{-1/2})$	$P_2(\text{m} \cdot \text{T}^{-(p+2)/2})$
19 July	$5.8 \pm 0.3 \cdot 10^{-19}$	$7.0 \pm 0.3 \cdot 10^{24}$

TABLE II: Results of P_1 and P_2 for the 19 July spectrum.

The 21 July 2013 spectrum was best explained by Razin effect alone with $p = 2.28 \pm 0.05$, $\nu_R = 0.44 \pm 0.04$ GHz and $P_1 = 1.18 \pm 0.05 \cdot 10^8 \text{ T}^{-(p+1)/2}$. The FFA+Razin fit had, as predicted, a $\chi^2 \sim 10^{-30}$, but was discarded because it gave a value for $p \sim 6$. Such a large p caused deviations of 1 or more orders of magnitude from the measured averages at 8.5 and 15 GHz.

The SSA+Razin model run out of time before reaching any result because the parameters used to initialise the fit were too far from the actual ones. In order to overcome this problem we fixed the first two parameters p and ν_R to the values found by Marcote et al. 2015 and scanned 3 orders of magnitude of the remaining 2-parameter space for values that would reduce χ^2 as much as possible. For the whole scanned space, χ^2 varied between 0.07 and 0.03, meaning that any convergence to the expected $\chi^2 = 0$ was slow. That explained why the fitting failed and also suggested that a vast region (at least 3 orders of magnitude in every parameter) of the 2-parameter space could produce an acceptable fit with a low value of χ^2 .

We then started a new fit from the best parameters we

had found. The fit was successful, but we kept plugging the obtained parameters as the starting point of the next fit to see if there was any stability to the solution. We consistently obtained the same values for $\nu_R = 0.44 \pm 0.01$ GHz and $p = 2.28 \pm 0.01$, the uncertainties accounting for the slight variations from fit to fit.

The ν_R obtained from SSA+Razin was the same as the pure Razin effect, confirming that SSA was not contributing significantly to the spectrum.

Spectrum	p	ν_R (GHz)
Average	2.16 ± 0.04	0.42 ± 0.02
19 July	1.86 ± 0.01	-
21 July	2.28 ± 0.05	0.44 ± 0.04

TABLE III: Results of the best fits for every spectrum. Razin for Average and 21 July, SSA for 19 July

VI. DISCUSSION AND CONCLUSIONS

We analysed the average spectrum of LS 5039 plus two simultaneous spectra in the 0.15-15 GHz range. We report a transition from an optically thin to optically thick source at ~ 0.5 GHz. The optically thin part is compatible with synchrotron emission with spectral index $\alpha = -0.58 \pm 0.02$. The optically thick part is best explained by Razin effect with $p = 2.16 \pm 0.04$ and $\nu_R = 0.42 \pm 0.02$ GHz.

The Razin effect has been detected and documented in colliding wind binaries (CWB) (Dougherty et al. 2003). This result further supports the non-accreting pulsar scenario because it could be compared to a CWB but with one of the members being a compact object emitting a weaker wind than its stellar companion.

The similarities between the pure Razin, SSA+Razin and FFA+Razin models for the average spectrum indicate that any absorption is hidden behind the cutoff pro-

duced by the Razin effect. That is, SSA or FFA must occur at lower frequencies than ν_R . In effect, the simultaneous spectra proved this (Fig. 5) and revealed a more dynamic picture of the radio source with it being capable of going from a pure SSA spectrum ($p = 1.86 \pm 0.01$) to Razin effect ($p = 2.28 \pm 0.05$, $\nu_R = 0.44 \pm 0.04$ GHz) in a timescale comparable to 1/2 orbital period. The variation of p between the simultaneous data suggests changes in the energy distribution of the injected electrons whereas variation in ν_R is tied to the electron density and the magnetic field.

Since the average spectrum comes from observations spread across the orbital phase and is close to the 19 July spectrum, it is reasonable to conclude that the source experiences the Razin effect most of the time and vanishes for short periods as seen in the 21 July spectrum.

Having said that, there are several ways to improve and get more significant results. First of all, measurements at lower frequencies are needed to better constrain all the parameters and potentially discard the FFA model if the measured data at ~ 0.1 GHz is close to the SSA and Razin fits in Fig. 4. Further measurements at 2.3 GHz are also needed to achieve a representative average of the flux at that frequency. To study orbital variations of the spectrum, more simultaneous spectra are needed. This would help to map where in the orbital phase the Razin effect becomes relevant and where it vanishes, which in turn could be used as an approximate map of the magnetic field or the electron density along the orbit.

Acknowledgments

I want to thank my advisor Josep Maria Paredes for his inputs and his help to make sure this is a good work. I also have to thank my friends who pushed me forward along the way during these last months.

-
- [1] Blackman, E. G., *Physics of Astrophysics I: Radiative Processes* [online] University of Rochester. New York, 2007. Lecture 22. Available at: <http://www.pas.rochester.edu/~blackman/ast461/lecture22.pdf>
 - [2] Casares, J., Ribó, M., et al. 2005, MNRAS, 364, 899
 - [3] Chernyakova, M., Malyshev, D., et al. 2019, A&A 631, A177
 - [4] Dougherty, S. M., Pittard, J. M., et al. 2003, A&A, 409, 217
 - [5] Dubus, G., 2013, A&A Rv, 21, 64
 - [6] ESA Gaia Archive, Early Data Release 3, 2020. Available at: <https://gea.esac.esa.int/archive/>
 - [7] Longair M. S., *High Energy Astrophysics*. (Cambridge University Press, Cambridge, 2011, 3rd ed.)
 - [8] Marcote, B., Ribó, M., Paredes, J. M., Ishwara-Chandra, C. H., 2015, MNRAS, 451, 59
 - [9] Paredes, J.M., Martí, J., Ribó, M., Massi, M., 2000, Science, 288, 2340
 - [10] Ricotti, M., *Plasma Effects* [online powerpoint] University of Maryland. Maryland, 2009. Available at: <https://www.astro.umd.edu/~ricotti/NEWWEB/teaching/plasma.pdf>
 - [11] Rybicki, G.B., Lightman, A.P., *Radiative processes in astrophysics*. (Wiley-Interscience, New York, 1979)
 - [12] Sarty, G. E., Szalai, T., et al. 2011, MNRAS, 411, 1293
 - [13] Zabalza, V., Bosch-Ramon, V., Aharonian, F., Khangulyan, D., 2013, A&A 551, A17